Carbon Nanoflask: A Mechanistic Elucidation of Its Formation

Rohit Kumar Rana and Aharon Gedanken*

Department of Chemistry, Bar-Ilan University, Ramat-Gan 52900, Israel

Received: January 28, 2002; In Final Form: May 20, 2002

A mechanistic detailed study on the formation of cobalt-encapsulating carbon nanoflasks is reported. Carbon nanoflasks were prepared from the decomposition products of $Co(CO)_3NO$, by carrying out the reaction in a specially arranged closed cell at 900 °C. The carbonaceous materials were separated from the product by a simple acid-treatment method. Structural and compositional analyses of the individual nanoflasks by selected area energy dispersive analysis by X-ray and selected area electron diffraction provided information about the formation mechanism of the cobalt filled nanoflasks. It was found that the Mg plays an important role by partially covering the cobalt particles. Over the exposed surfaces of these cobalt particles, nanotubes are nucleated via a CO decomposition reaction, which is believed to be promoted by Mg. Since the attached cobalt particles are comparatively bigger than the tubular part, the appearance of a nanoflask is obtained.

1. Introduction

The remarkable C_{60} discovery in 1985[1] led to an explosion of research into carbon science for the past few years. Among others, the most notable finding was the multitude of novel shapes that carbon could adopt under different processing conditions in an arc discharge chamber.[2] Particularly, it is extremely intriguing to note the effect that different metals imparted on the intricate microstructure of carbon. Structures such as sea urchins (catalyzed by Gd), bamboo trunks, and necklaces (catalyzed by Ni) were some of the more fascinating microstructures to emerge from the interaction of carbon and metals in the vapor phase.[3−5] While most of the experiments generated curved carbon morphology, the reaction with the alkaline earth metals (Ca, Sr) resulted in cubes of carbon nanocages[5] with sharp edges. There are even reports where nanocarbons shaped as cones were generated without the aid of any metal.[7,8]

In 1991, another extremely exciting form of pure carbon, the carbon nanotubes, was detected by Iijima[9] while examining the soot obtained from the cathodic deposit of an arc-discharge fullerene production apparatus. Investigations of nanotube production through the catalytic decomposition of carbon-containing gases resulted in several more interesting morphologies such as curled, hemitoroidal, branched, and spiral- and helix-shaped nanotubes and nanofibers, besides the straight ones.[10] From the early studies of carbon filaments, it is known that the change in parameters, such as the type of hydrocarbon, catalysts, particle size, and temperature, can lead to different tubular structures or filaments possessing various morphologies and degree of graphitization.[10] The detailed structure of these forms of carbon was investigated by various techniques, and it was found that extremely marked physical differences could be encountered in the nanofibers that were entirely dependent on the chemical nature of the catalyst.[11] Careful examination indicated that most of these morphologies were determined by the physical shape adopted by the catalyst. Kim et al.[12] observed a bidirectional growth of carbon nanofibers from two opposite faces of the catalyst particle. In some cases, the catalyst particles were observed to execute a rotary motion and this action resulted in nanofibers acquiring a twisted form or helical structure.[13] Branched nanofibers were produced when a catalyst particle located at the growing end of a whiskerlike structure suddenly "exploded" into numerous smaller particles, each of which then proceeded to generate secondary smaller nanofibers.[14] Under different conditions helix-shaped graphite nanotubes were obtained by a catalytic pyrolysis of acetylene.[15] Amelinckx and co-workers[16] described this spiral growth process by invoking the concept of the spatial−velocity hodograph related to anisotropy growth rates that leads to a rotating growth front.

Our experiments with the catalytic formation of carbon nanotubes gave rise to yet another unique morphology resembling the shape of a flask.[17,18] A nanoflask can be described as having a globular base, to which the narrower tubular part is attached, giving it the shape of a flask. More importantly, the metal catalyst was found encapsulated within the globular end of the nanoflask. These structures were produced by a catalytic method, where the catalyst and the carbon sources were generated in situ by decomposing $Co(CO)_3NO$ at 900 °C in a closed container. Because of the attached cobalt particles, it was possible to separate them from other unwanted materials by simply applying a magnet. This enriched product was then used to study the magnetic behavior of the encapsulated metal.[18] It is anticipated that with the help of a magnet these nanoflasks can also be aligned on a flat surface. The unique structure of nanoflasks may lead to a range of different properties by enclosing various other metals or alloys inside the cavity. However, for any practical use of these materials, the production method has to be improved in both quantity and quality, which requires a thorough understanding of their formation mechanism. Here we report a detailed study on the synthesis and formation mechanism of the cobalt encapsulated carbon nanoflasks based on our new experimental data.

2. Experimental Section

In our experiment of nanoflask preparation, we use Mg powder treated with a mixture of ethanol and water instead of pure Mg powder or turnings as one of the reactants, apart from

* To whom correspondence should be addressed. Fax: +972-3-5351250. E-mail: gedanken@mail.biu.ac.il.

10.1021/jp025566j CCC: $22.00
Published on Web 08/23/2002

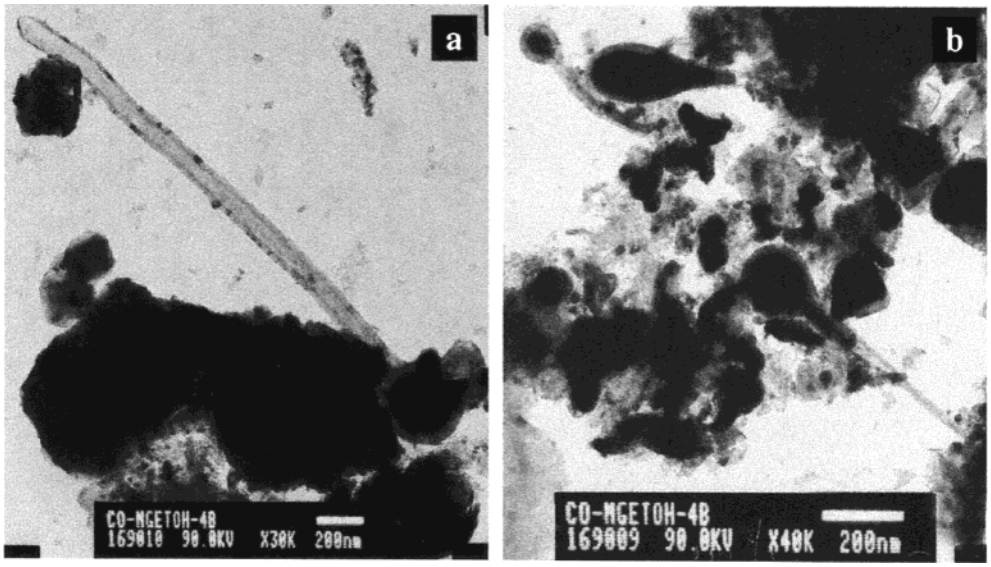

Figure 1. TEM images of the nanoflasks in (a**)** the as-synthesized sample and **(**b**)** a sample separated from the as-synthesized material with the help of a magnet.

$Co(CO)_3NO$. This is based on the fact that nanoflasks were obtained only when the Mg powder (old stock) was used rather than the Mg turnings (freshly obtained). This prompted us to analyze the differences between the two types of Mg (freshly obtained turnings and old powder). X-ray diffraction (XRD) of the two samples clearly showed that the Mg powder (old) has peaks due to the presence of $Mg(OH)_2$ along with Mg peaks, whereas the Mg turnings showed only Mg peaks. It has also been reported[19] that the as-received commercial Mg metal normally contains a surface covered by a film constituted of mainly magnesium hydroxide and a smaller quantity of magnesium bicarbonate, as revealed from XPS measurements. So, to understand the role of $Mg(OH)_2$ in the formation of a nanoflask, freshly obtained Mg powder was treated with a mixture of ethanol and water to give an outer $Mg(OH)_2$ layer surrounding the Mg core (denoted as Mg-EtOH). This sample was vacuum-dried to get a gray colored powder, which was then used in the reaction along with $Co(CO)_3NO$ as described below.

Synthesis of the carbon nanoflask was carried out in a 2 mL closed cell, which was assembled from stainless steel Swagelok parts. A 3/8• union part was capped from one side by a standard plug. In a typical preparation method, 400 mg of Mg-EtOH powder was inserted into the cell, and 700 mg of cobalt tricarbonyl nitrosyl (STREM) was then added to it slowly by a syringe. All the materials were loaded into the swagelok cell in an inert atmosphere of nitrogen (glovebox). The filled cell was closed tightly by the other plug and then heated in a furnace to 900 °C at a heating rate of 20 °C/min. The reaction was continued for 3 h, after which the cell was cooled to room temperature. The as-synthesized black product obtained from the cell was treated with 30% dilute HCl solution in order to remove the catalytic particles. The resulting purified material was centrifuged, repeatedly washed with deionized water and ethanol, and then vacuum-dried.

The X-ray diffraction patterns of the products were recorded by employing a Bruker AXS D8 advanced powder X-ray diffractometer (using Cu Kα $\lambda = 1.5418$ Å radiation). The transmission electron micrographs (TEM) were obtained with a JEOL-JEM 100SX microscope, working at a 100 kV accelerating voltage. Samples for TEM were prepared by dispersing the powdered sample in ethanol by sonication and then drop-drying on a copper grid (400 mesh, Electron Microscopy Sciences) coated with carbon film. High-resolution TEM (HRTEM) images were obtained from a Philips CM-120 instrument. Selected area electron diffraction (SAED) and selected area energy dispersive analysis by X-ray (SAEDAX) were carried out with the respective analyzers attached with the HRTEM instrument. Elemental analysis was done by an Eager 200 CHN analyzer.

3. Results

3.1. XRD Analyses. The structural determinations of various components in the as-synthesized and acid-treated samples were done by XRD. As has been previously reported,[17] the as-synthesized sample mainly consists of MgO, metallic cobalt particles, and graphite. Acid treatment of the sample resulted in the removal of catalytic particles, making the (002) graphitic peak more prominent. From the graphitic (002) peak the average interlayer spacing was calculated to be of 3.4 Å. The Co particles were found to be in their metastable FCC phase even after the acid treatment. The stabilization of the FCC structure rather than the stable HCP phase is similar to our earlier report,[17] where the covering graphene layers have been proposed to be responsible for such a phenomenon.

3.2. CHN Analyses. Carbon contents in various samples were determined by CHN analysis. The as-synthesized sample obtained after 3 h of reaction showed a carbon content of 11.4 wt %. In good agreement with this, the amount of material that was recovered from the products after treating with HCl corresponded to about 10.6 wt % of the as-synthesized product. The balance of weight shows the effectiveness of the purification method, which caused removal of the catalytic materials only. On the other hand, the acid-treated sample showed a carbon content of 89 wt %, and the contents of H, N, and O were below 1 wt %.

3.3. TEM Analyses. Representative TEM images of the as-synthesized and the extracted products are illustrated in Figures1 and 2, respectively. As seen in Figure 1a,b, the catalytic particles were detected in the as-synthesized material, along with carbon nanoflasks. However, these impurities were not seen after HCl treatment of the product, and the nanoflasks were clearly visible, as shown in Figure 2. The morphologies of the nanotubes before and after the acid treatment remained similar, indicating that they are undamaged by this purification method.

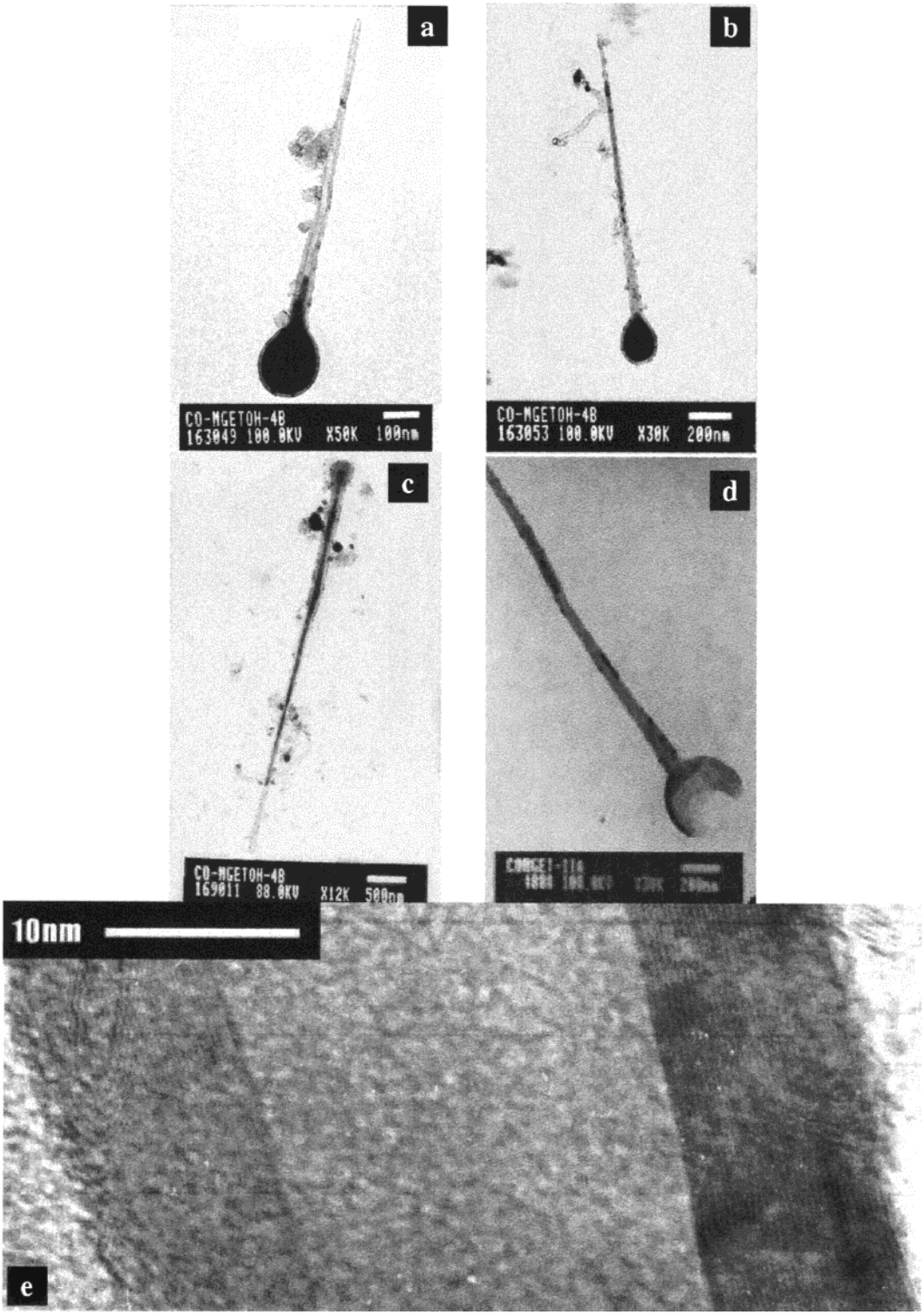

Figure 2. TEM images of the nanoflasks in the acid-treated sample: (a,b) globular part of the nanoflasks filled with cobalt; (c) a complete filling of the nanoflask by cobalt; (d) an incompletely formed nanoflask, and **(**e**)** HRTEM of the tubular part of the nanoflask shown in Figure 3.

The dimensions of these nanoflasks vary over a wide size range. Almost all the nanoflasks were constructed of a straight tubular part commencing from a relatively bigger globular base. The diameter of the tubular part was found to be not uniform throughout the tube. From the neck to the tail there is a gradual decrease in the diameter. The length of the tubular parts was sometimes found to extend up to few micrometers. The size of the globular part of the nanoflasks was widespread from 50 to 900 nm. In most cases, the cobalt metal was detected within the globular part of the nanoflasks, while a few had an empty core. The empty core might be a result of the removal of metal particles during the acid-treatment procedure. For the encapsulated particles, the metal was well-protected by the surrounding graphene layers from leaching out by the acid. In Figure 2e, the HRTEM image of the tube confirms the presence of multilayered graphene layers arranged along the tube axis. In a few cases, a complete filling of the metal throughout the tube, or at least up to the neck, was observed, as shown in Figure 2c. In some cases, incomplete nanoflasks of the type shown in Figure 2d were also noticed.

Figure 3. Representative TEM image of an individual nanoflask present in the as-synthesized sample on which SAED and SAEDAX analyses were performed.

3.4. SAEDAX and SAED. To clarify the exact role played by the catalyst on the nanoflask formation, we made an effort to characterize individual nanoflasks before the acid treatment. Compositional and structural information on the individual nanoflasks were obtained by SAEDAX and SAED analyses on various selected areas of the nanoflask. Figure 3 illustrates a representative TEM image of two such nanoflasks, which were chosen for the study. Analyses were done from three different parts, such as the globular base, neck, and tubular tail of the nanoflask. The SAEDAX scan from the globular part is shown in Figure 4a. Besides the presence of carbon and cobalt, an appreciable amount of magnesium was detected in the globular part. On the other hand, the SAEDAX analyses from the neck and tail parts of the nanoflask revealed that they are composed solely of carbon. A typical SAEDAX scan obtained from the neck is shown in Figure 4b. The atomic percentages of various elements in different parts of the nanoflask are summarized in Table 1. Compositions of the two chosen nanoflasks were similar, and no obvious differences among them were detected, except for detection of a small amount of oxygen in one case. The presence of oxygen may be a result of the exposure of Mg to air/moisture during the sample preparation for TEM measurements.

To get the structural information, SAED was done on the globular part from which the SAEDAX results were collected.

TABLE 1: Elemental Composition of the Globular Part of the Two Individual Nanoflasks as Calculated from SAEDAX Analyses

	at. %	
element	nanoflask-1	nanoflask-2
C	36.9	33.1
O	3.2	--
Mg	12.3	13.8
Co	47.6	53.0

The SAED pattern from the globular part is shown in Figure 5. They were analyzed by considering the various elements that were detected by SAEDAX. The brightest innermost ring corresponds to 002 reflection of hexagonal graphite. Clear spots were seen for the other graphitic reflection from 100 planes. The observation of the 002 ring and spots for 100 reflections suggest that the graphitic wall consist of 002 planes perpendicular to the beam direction. The calculated $d(002)$ value of 3.41 Å is 0.03 Å less than the reported value for carbon nanotube/nanoparticle mixtures obtained by the arc-discharge method.[20] However, it is known from the more recent analysis by Kiang et al.[21] that the interlayer spacing can vary from 3.4 to 3.9 Å, depending on the tube diameter, with the smaller diameter tubes having the largest spacing. This correlation was attributed to the high curvature of the small tubes resulting in a greater repulsive intertube force.

The other sharp spots could be identified as reflections from FCC cobalt and hexagonal magnesium. A comparison of the interlayer distances measured by electron diffraction with the known values is presented in Table 2. The diffraction pattern from FCC cobalt corresponds with a [011] zone-axis pattern. The FCC phase of the cobalt confirms the XRD results that the metastable high-temperature FCC phase of cobalt is protected by the surrounding graphene layers. The presence of metallic Mg, however, could not be observed by XRD, probably because of the smaller amount that is below its detection limit. But, the appearance of clear spots for both cobalt and magnesium indicates that the metals are highly crystalline with some preferred orientations.

4. Discussion

The mechanism of the formation of carbon nanotubes and filaments has been the subject of many studies in the past few years. The early model was the result of extensive work by Baker and co-workers.[22] In their proposed mechanism, the key steps are the adsorption and decomposition of a hydrocarbon on a metal surface to produce carbon species, which dissolve and diffuse through the bulk and ultimately precipitate at the rear of the particle to form nanofiber. In a more recent work,

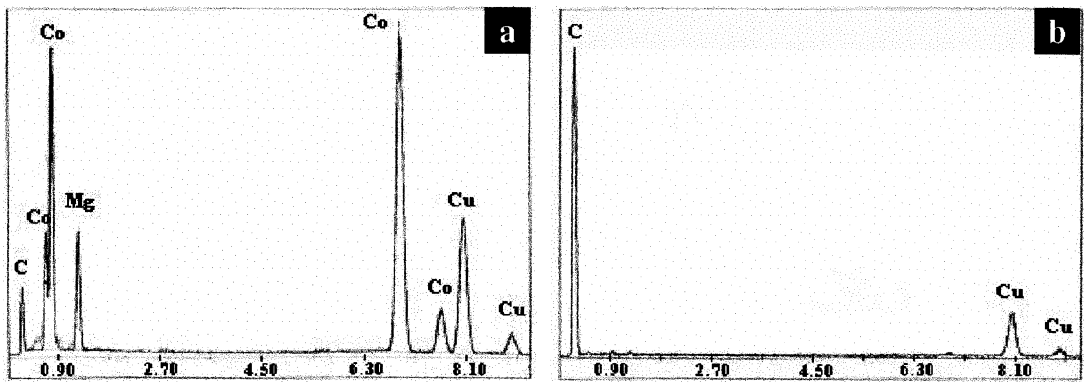

Figure 4. SAEDAX scan obtained from (a**)** the globular and **(**b**)** the neck part of the nanoflask shown in Figure 3. The Cu peaks are due to the copper support grid.

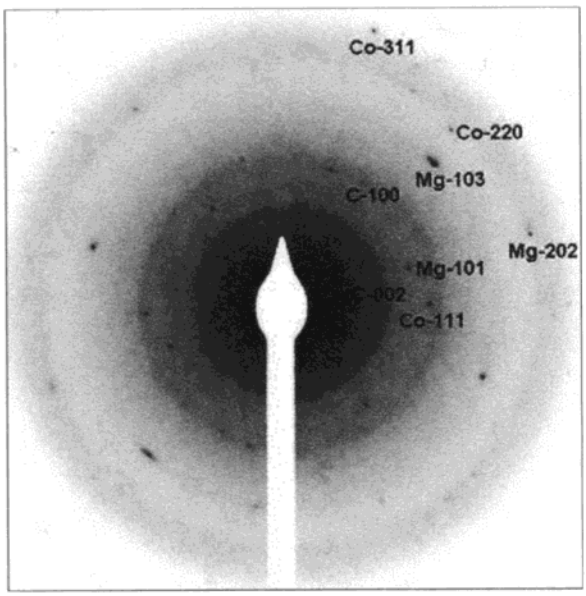

Figure 5. SAED pattern obtained from the globular part of the nanoflask shown in Figure 3.

TABLE 2: Summary of SAED Data Recorded from the Globular Part of the Nanoflasks

measd "*d*" (±0.03 Å)	known "*d*"[a] (nm)	assigmt (*hkl*)
3.41	3.376	C (002)
2.42	2.452	Mg (101)
2.16	2.139	C (100)
2.08	2.047	Co (111)
1.49	1.473	Mg (103)
1.26	1.253	Co (220)
1.21	1.226	Mg (202)
1.04	1.069	Co (311)

[a] The interplanar distance, "*d*" values are from JCPDS files: C (41-1487), Mg (35−821), and Co (15−806).

Dai et al.[23] prepared single-walled carbon nanotubes by CO disproportionation catalyzed by Mo particles. For this they proposed another mechanism,[24] according to which an excess of carbon initially assembles on the metal particle surface to form a graphene cap (so-called "Yarmulke") with its edge strongly chemisorbed to the metal. The newly arriving carbon atoms then either form another cap underneath the first or add to the cylindrical section of the growing layer. A crucial feature of the Yarmulke mechanism is the avoidance at all stages of the growth of any open edges, which would expose energetically costly dangling bonds. It should be noted, however, that in all the proposed mechanisms, the diameter of the nanotube or nanofiber is governed by the size of the associated catalyst particles. The nature of the catalyst (supported or unsupported) and the temperature at which the reaction is conducted influence the size of the metal particles, which in turn controls the diameter of the generated tubes. But, as far as the nanoflasks are concerned, it is clearly an exceptional case where the attached particles are larger than the tubular part and which causes its unique shape. To rationalize such a deviation from the normal phenomenon, a possible mechanism for the nanoflask growth has been put forward as discussed in the following sections.

4.1. Chemical Reaction. Liu et al.[17] proposed a possible reaction mechanism for the nanoflask formation, where the "carbon nanoflasks" were believed to be formed as a result of CO reduction by Mg. This mechanism was based on the fact that the final product contained the oxidized product of Mg. Moreover, the thermodynamics of the reaction strongly favor this reduction mechanism. For example, the $\Delta G°$ for the above reaction ($Mg + CO \rightarrow C + MgO$) at 900 K and 1 atm is −313.4 kJ/mol in contrast to −12.9 kJ/mol for the alternative process involving the CO disproportionation reaction ($2CO \rightarrow C + CO_2$). However, since the used Mg (old) in the above experiment was already contaminated with $Mg(OH)_2$ (see Experimental Section), the formation of MgO must be a result of the reaction of Mg with $Mg(OH)_2$ or a decomposition product of $Mg(OH)_2$. XRD analyses of the magnesium powder used in the previous experiments revealed a rather appreciable content of $Mg(OH)_2$ corresponding to ∼15% of the total weight. Moreover, the presence of air/moisture while loading the reactants inside the cell might also have converted some of the Mg to MgO.

Now the question is whether the reaction for "carbon nanotube" formation proceeds through the "CO reduction by Mg" or "CO disproportionation reaction". To clarify the above doubt, a reaction was carried out in an inert atmosphere of nitrogen and fresh Mg turnings were used instead of Mg (Old) powder. The result showed only a few carbon nanotubes along with the MgO and Mg present in the product. The fact that MgO was found in the product means that the reaction of Mg with CO forming "carbon" cannot be completely ignored. But, as far as the carbon nanotubes and carbon nanoflasks are concerned, they were often found attached with cobalt particles at one end of the tube, which clearly indicates that their formation is catalyzed by the cobalt particles. To get more insight into the reaction pathway, additional information was obtained from an experiment where the $Co(CO)_3NO$ was decomposed over a MgO powder instead of Mg metal in a closed cell.[25] This reaction also yielded carbon nanotubes, and more importantly, the amount was much higher than that obtained from the reaction with fresh Mg turnings. This certainly indicates that the nanotube formation does not require the presence of Mg. So, clearly the other possible path for the nanotubes and, in particular, nanoflasks formation in the present case, is the so-called "Boudouard reaction," which involves the disproportionation of CO catalyzed by cobalt. However, the possibility of carbon nanotube formation via the CO reduction by Mg cannot be entirely ruled out for reasons that are discussed elsewhere.[26]

4.2. Mechanism. To develop a comprehensive understanding of the growth mechanism, it is essential to consider the various processes that are eventually taking place with a gradual increase in temperature while heating the cell. The first step that one can expect is the reaction of Mg metal with $Mg(OH)_2$, producing MgO. This MgO acts as a support for the dispersion of cobalt particles formed from the decomposition of $Co(CO)_3NO$. Since the surface area of the Mg-EtOH powder is much smaller compared to the commercially available MgO (4 vs 52 m^2/gm), it can only give rise to a low dispersion of cobalt particles resulting in the formation of bigger particles of 50−900 nm sizes. Then, when the temperature reaches the melting point of Mg (650 °C), the remaining Mg metal can diffuse through the MgO outer layer and cover fully or partially from the sides the Co particles laying over the MgO surface. This is based on the EDX and SAED results obtained from individual carbon nanoflasks, which showed the presence of Mg only in the globular part of the nanoflask. A schematic picture of the mechanism involved in the nucleation and growth process of carbon nanoflasks is illustrated in Figure 6.

4.2.1. Nucleation and Growth. As the temperature further increases, CO disproportionates over only those cobalt particles that have exposed surface, i.e., those that are not fully covered by Mg. The generated carbon then initially dissolves inside

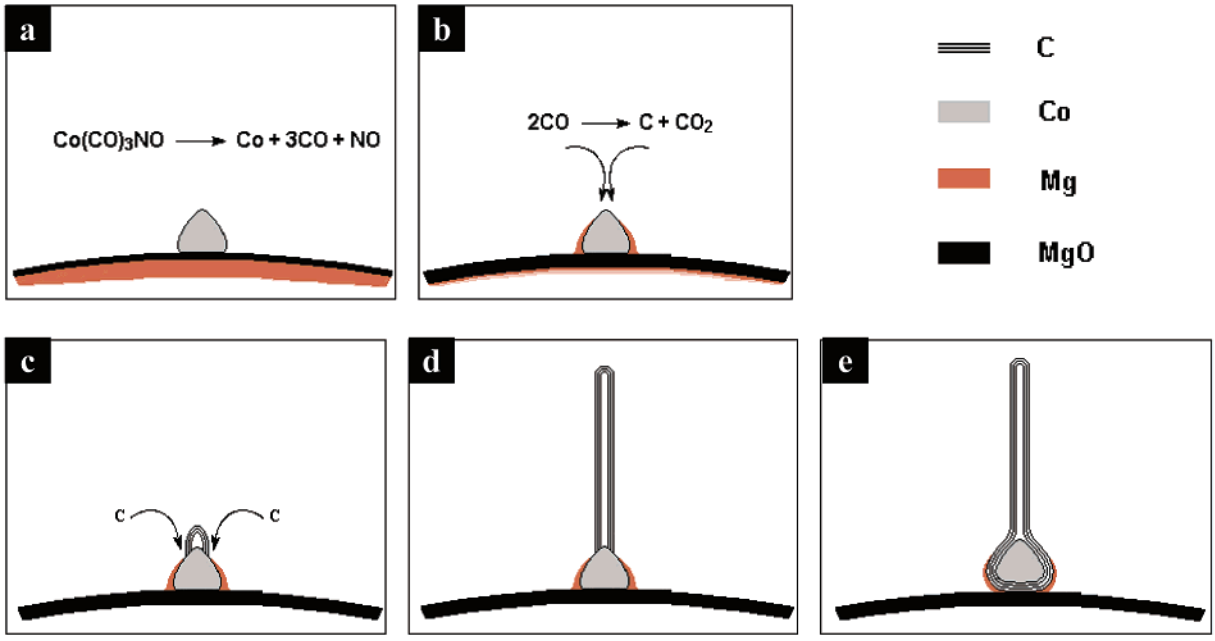

Figure 6. Schematic representation of various steps involved in the carbon nanoflask growth process. (a) Decomposition of $Co(CO)_3NO$ generates cobalt particles over a MgO support; (b) as the temperature increases, Mg melts and partially covers the cobalt particle; (c) over the exposed part of this cobalt particle CO disproportionates to form carbon and accumulation of carbon forms a graphitic cap attached to the cobalt particle; (d) as the cap grows further, a tube is generated; (e) termination of the growth process after the graphene layers completely cover the catalyst.

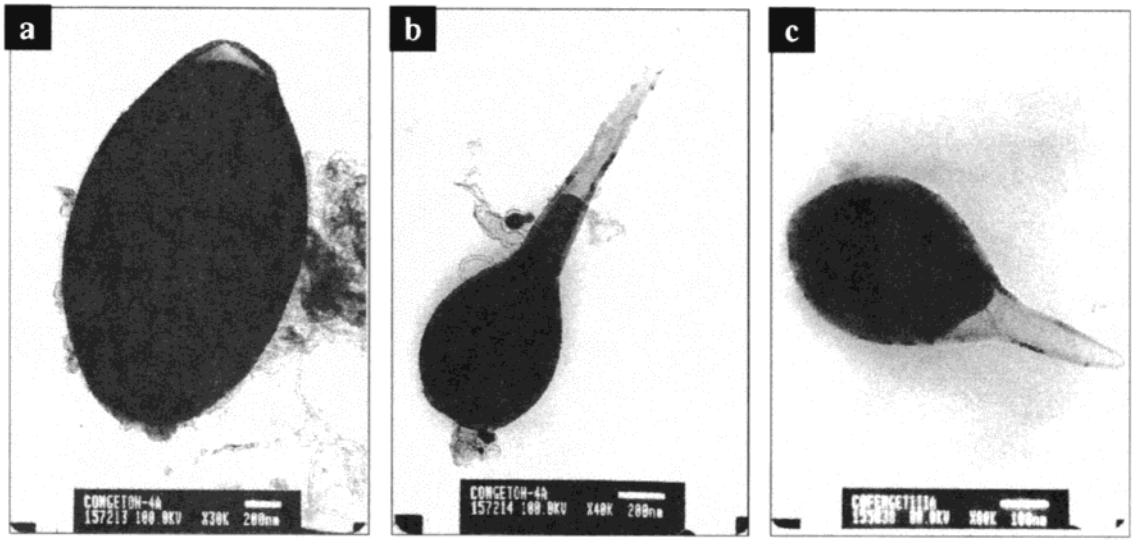

Figure 7. TEM images depicting the initial growth stages involved in the formation of nanoflask.

cobalt, as has been proposed for the catalytic formation of carbon nanotubes.[10] When the metal gets supersaturated with carbon, it tries to precipitate out as graphene layers over the exposed surface of the cobalt particle, forming the so-called Yarmulke[24] (Figure 6c). The graphene layers then grow upward as additional carbon atoms are being added to the cylindrical part. Thus a hollow tube is created over the exposed part of the cobalt particle. It is obvious that the possibility for such a process to occur will depend on processes at the interface between the carbon containing gas and the exposed part of the metal. The TEM images shown in Figure 7 depict the different growth stages of nanoflask formation, consistent with the above proposed growth mechanism.

As seen in Figure 2c, the complete filling of the tube or filling until the neck by the metal indicates that at a certain time the metal probably gets enough fluidity to flow through the tube as a result of capillary action. The presence of the liquid form of the metal during the carbon nanotube growth has already been predicted in earlier works.[22] Such an assumption is consistent with the frequently observed droplet-like shapes of the attached metal catalyst, which can only be explained if the particles have previously been in the liquid state.[27] On the basis of this observation, a VLS (vapor−liquid−solid) mechanism for the nanotube growth was proposed,[27] according to which the liquid metal catalyst accepts material from the vapor, causing the liquid to become supersaturated. An interfacial energy contribution to the total free energy of the particles was believed to be responsible for such a decrease in the melting temperature of the metal catalyst.

However, it should be pointed out here that the bigger metal particles (>100 nm) are generally known to favor carbon encapsulation rather than the nanotube formation. This argument is based on the fact that the strain energy of the overcoating layer becomes smaller as the metal particle becomes bigger.[24] But in our case, though the partially covered particles are bigger, they act like a suitable catalyst for the nanotube formation, where

the nanotube grows from the exposed part of the particle in a manner similar to that in the case of smaller particles. It seems that the small exposed surface of these partially covered particles mimic the activity of the smaller particles which is generally necessary for the nanotube formation. We believe that a promotional effect of Mg on the cobalt particles may be responsible for such an activity. This is based on our previous studies on the decomposition of $Co(CO)_3NO$ over a mixture of Mg and MgO.[25] It was found that the use of Mg along with MgO increases the carbon yield by twice the value obtained when only MgO is used as the support. This clearly suggests that the magnesium plays an important role in CO disproportionation reaction.

It is likely that Mg can promote the CO dissociation reaction in a similar manner as known in the case of alkali-promoted Fischer−Tropsch catalysis.[28] It has also been demonstrated that even the single crystals of transition metals are active enough to catalyze the CO hydrogenation in a manner similar to that by the nanoparticles.[29] From the early works on carbon filaments, it has also been found that the activity of transition metals toward the formation of carbon nanostructures can be greatly enhanced by addition of an adatom, which can either be another metal (Cu, Sn, K) or a nonmetal (S).[30] Various experiments and theoretical calculations have shown that the interaction of electropositive adatoms such as Na or K with the transition metal surface causes an enhancement of the binding energy of molecularly adsorbed CO and increases the dissociation probability of CO.[28,29] This has been attributed to the increased electron density on the transition metal surface atoms by the adsorption of alkali metal atoms on them. On the other hand, Mg may also indirectly promote the cobalt catalyst through an interaction with the MgO support. It has been shown that when MgO is exposed to Mg vapor, it generates an electron-rich surface by creating defect centers consisting of single electrons in anionic vacancies.[31] These electron rich defect sites can activate the cobalt catalyst by donating electrons through a metal/support interaction.

4.2.2. Termination. The TEM observations clearly reveal that the cobalt particles present at the end of the nanoflasks are covered with graphene layers. Once these catalytic particles are fully covered with carbon, the further growth of the attached nanotube stops. But, the central importance is the mechanism by which the graphene layers are formed over the metal. It has been argued that the encapsulation of the metal takes place once the catalyst becomes bigger because of accretion of metal atoms from the gas phase onto the metal particle.[24] But in our case, the metal particles are already big enough, and, moreover, there is no probability for the further growth of particle size as the entire cobalt carbonyl complex might have already been decomposed completely. Since the cobalt particles are covered with Mg on one part and the nanotube is covering the other part, the formation of encapsulating graphene layers is only possible in an "inside-out" direction. According to the previous discussion, during the time in which the particle is active, it accumulates a large concentration of carbon atoms prior to the nanotube nucleation. Since the encapsulated cobalt particles have been found to exhibit no carbide peaks in XRD and SAED, it indicates that the excess carbon does not stabilize as carbide within the particle. So, once the temperature is lowered, these carbon atoms have to separate out of the metal, which results in forming the encapsulating graphene layers and simultaneously pushes away the outer Mg covering (Figure 6e). A similar kind of inside-out mechanism has also been considered by Bladh et al.,[32] in order to explain the formation of carbon encapsulated iron particles from a CO disproportionation reaction. If the amount of carbon atom is insufficient for complete covering, one might expect the formation of partially covered metal particle. In fact, this is supported by our observation of incomplete nanoflasks (Figure 2d), where the metal has been removed by reacting it with HCl through the uncovered portion. It is also expected that the sites where tubes are attached with the metal may provide the nucleating points for the formation of surrounding graphene layers.

5. Conclusions

The above analysis considers possible chemical reaction and different growth stages for the cobalt encapsulated nanoflask formation. It was found that the presence of Mg is critical to the nanoflask formation. The resulting nanoflasks and the novel growth process may have important bearing on creation of other types of nanomaterials. There has been substantial recent interest in filled nanotubes. The nanoflasks may be a convenient system for such studies, where efforts are now being made to incorporate various other useful nanomaterials. Combined with the mechanically robust tubular part, it is expected that these encapsulated materials may exhibit interesting properties for various applications.

Acknowledgment. We thank the Israeli Ministry of Science, Culture, and Sports for supporting this research via an Infrastructure grant. R.K.R. thanks the Bar-Ilan Research Authority for his postdoctoral fellowship. A.G. thanks the German Ministry of Science through the Deutsche-Israel program, DIP, for its support. The authors are grateful to Prof. Z. Malik, Faculty of Life Sciences, for extending to us the use of their facilities.

References and Notes

(1) Kroto, H. W.; Heath J. R.; O'Brien, S. C.; Curl, R. F.; Smalley, R. E. *Nature* **1985**, *318*, 162.

(2) Osawa, E.; Yoshida, M.; Fujita, M. *MRS Bull.* **1994**, *19*, 33.

(3) Subramoney, S.; Ruoff, R. S.; Lorrents, D. C.; Malohotra, R. *Nature* **1993**, *366*, 637.

(4) Saito, Y.; Yoshikaya, T. *J. Cryst. Growth* **1993**, *134*, 135.

(5) Seraphin, S.; Zhou, D.; Jiao, J.; Minke, M. A.; Wang, S.; Yadav, T.; Withers, J. C. *Chem. Phys. Lett.* **1994**, *217*, 191.

(6) Saito, Y.; Matsumoto, T. *Nature* **1998**, *392*, 237.

(7) Ge, M.; Sattler, K. *Chem. Phys. Lett.* **1994**, *220*, 192.

(8) Krishnan, A.; Dujardin, E.; Treacy, M. M.; Hugdahl, J.; Lynum, S.; Ebbesen, J. W. *Nature* **1997**, *388*, 451.

(9) Iijima, S. *Nature* **1991**, *354*, 56.

(10) (a) Rodriguez, M. M. *J. Mater. Res.* **1993**, *8*, 3233. (b) De Jong, K. P.; Geus, J. W. *Catal. Rev.−Sci. Eng.* **2000**, *42*, 481.

(11) Audier, M.; Oberlin, A.; Oberlin, M.; Coulon, M.; Bonnetain, L. *Carbon* **1981**, *19*, 217.

(12) Kim, M. S.; Rodriiguez, N. M.; Baker, R. T. K. *J. Catal.* **1991**, *131*, 60.

(13) Baker, R. T. K.; Barber, M. A.; Harris, P. S. *Nature* **1975**, *253*, 37.

(14) Baker, R. T. K.; Chludzinski, J. J. *J. Catal.* **1980**, *64*, 464.

(15) Ivanov, V.; Nagy, J. B.; Lambin, P.; Licas, A.; Zhang, X. B.; Zhang, X. F.; Bernaerts, D.; Van Tendeloo, G.; Amenickx, S.; Van Landuyt, J. *Chem. Phys. Lett.* **1994**, *223*, 329.

(16) Amelinckx, S.; Zhang, X. B.; Bernaerts, D.; Zhang, X. F.; Ivanov, V.; Nagy, J. B. *Science* **1994**, *265*, 635.

(17) Liu, S.; Tang, X.; Yin, L.; Koltypin, Y.; Gedanken, A. *J. Mater. Chem.* **2000**, *10*, 1271.

(18) Liu, S.; Boeshore, S.; Fernandez, A.; Sayagues, M. J.; Fischer, J. E.; Gedanken, A. *J. Phys. Chem. B* **2001**, *105*, 7606.

(19) Abreu, J. B.; Soto, J. F.; Facey, A. A.; Soriaga, M. P.; Garst, J. F.; Stickney, J. L. *J. Colloid Interface Sci.* **1998**, *206*, 247.

(20) Saito, Y.; Yoshikawa, T. *Phys. Rev. B* **1993**, *48*, 1907.

(21) Kiang, C.-H.; Endo, M.; Ajayan, P. M.; Dresselhaus, G.; Dresselhaus, M. S. *Phys. Rev. Lett.* **1998**, *81*, 1869.

(22) (a) Baker, R. T. K.; Barber, M. A.; Harris, P. S.; Feates, F. S.; Waite, R. J. *J. Catal.* **1971,** *26*, 51. (b) Baker, R. T. K.; Harris, P. S.; Thomas, R. B.; Waite, R. J. *J. Catal.* **1973**, *30*, 86.

(23) Dai, H.; Hafner, J. H.; Rinzler, A. G.; Colbert, D. T.; Smalley, R. E. *Nature* **1996**, *384*, 147.

(24) Dai, H.; Rinzler, A. G.; Nikolaev, P.; Thess, A.; Colbert, D. T.; Smalley, R. E. *Chem. Phys. Lett.* **1996**, *260*, 471.

(25) (a) Rana, R. K.; Koltypin, Y.; Gedanken, A. *Chem. Phys. Lett.* **2001**, *344*, 256. (b) Rana, R. K.; Xu, X. N.; Yeshurun, Y.; Gedanken, A. *J. Phys. Chem. B* **2002**, *106*, 4079.

(26) Motiei, M.; Hacohen, Y. R.; Calderon-Moreno, J.; Gedanken, A. *J. Am. Chem. Soc.* **2001**, *123*, 8624.

(27) Kukovitsky, E. F.; L_vov, S. G.; Sainov, N. A. *Chem. Phys. Lett.* **2000**, *317*, 65.

(28) (a) Dry, M. E.; Shingles, T.; Van H. Botha, C. S. *J. Catal.* **1970**, *17*, 341. (b) Kiskinova M. P. *Surf. Sci.* **1981**, *111*, 584. (c) Jenkins, S. J.; King, D. A. *J. Am. Chem. Soc.* **2000**, *122*, 10610.

(29) (a) Crowell, J. E.; Garfunkel, E. L.; Somorjai, G. A. *Surf. Sci.* **1982**, *121*, 303. (b) Campbell, C. T.; Goodman, D. W. *Surf. Sci.* **1982**, *123*, 413.

(30) (a) Boehm, H. *Carbon* **1973**, *11*, 583. (b) Benissad, F.; Gadelle, P.; Coulon, M.; Bonnetain, L. *Carbon* **1989**, *27*, 585. (c) White, R. B. U.S. Patent 2621216, Dec 9, 1952. (d) Gardner, D. G.; Bartholomew, C. H. *Ind. Eng. Chem. Prod. Res. Dev.* **1981**, *20*, 80.

(31) (a) Giamello, E.; Murphy, D.; Ravera, L.; Coluccia, S.; Zecchina, A. *J. Chem. Soc., Faraday Trans.* **1994**, *90*, 3167. (b) Giamello, E.; Ferrero, A.; Coluccia, S.; Zecchina, A. *J. Phys. Chem.* **1991**, *95*, 9385.

(32) Bladh, K.; Falk, L. K. L.; Rohmund, F. *Appl. Phys. A* **2000**, *70*, 317.